Ultrafine MOF as charge trap enables superior high-temperature energy storage performance in polyetherimide composites dielectrics

Na Zhang, Hang Zhao, Chuying Zhang, Haotong Guo, Zhi-Min Dang, Jinbo Bai

Ultrafine MOF as Charge Trap Enables Superior High-Temperature Energy Storage Performance in Polyetherimide Composites Dielectrics

Na Zhang[1], Hang Zhao[1]*, Chuying Zhang[1], Haotong Guo[1], Zhi-Min Dang[2]*, and Jinbo Bai[3]*

[1]*International Collaborative Center on Photoelectric Technology and Nano Functional Materials, and Institute of Photonics & Photon-Technology, Northwest University, Xi'an 710069, P. R. China*

[2]*State Key Laboratory of Power System, Department of Electrical Engineering, Tsinghua University, Beijing 100084, P. R. China*

[3]*Université Paris-Saclay, CentraleSupélec, ENS Paris-Saclay, CNRS, LMPS-Laboratoire de Mécanique Paris-Saclay, 8-10 rue Joliot-Curie, Gif-sur-Yvette 91190, France*

[*]*Correspondence:hang.zhao@nwu.edu.cn; dangzm@tsinghua.edu.cn; jinbo.bai@centralesupelec.fr*

Abstract

Polymer dielectrics are crucial for electrostatic energy storage and offer broad application prospects in advanced high-power electrical systems, but their energy storage performance declines considerably due to increased conductivity at elevated temperatures. This work presents a structurally-simple high-temperature composite dielectric by incorporating positively charged ultrafine UIO-66 nanoparticles into polyetherimide (PEI)

matrix. Be distinguished from traditional sub-micron MOF structures that usually reported in very recently, the newly-found nanoscale effect endows the ultrafine UIO-66 (~12.9 nm) with largely-increased active sites, surface charge density and electron affinity. These ultrafine UIO-66 nanoparticles can capture free charge through strong electrostatic interactions and introduce deeper traps in composite dielectrics, reducing conduction loss and improving energy storage property significantly at elevated temperatures. Specifically, filling only as tiny as 0.5 wt% ultrafine UIO-66 endows the PEI-based composite with ultra-high energy densities of 5.9 J cm^{-3} and 3.7 J cm^{-3} accompanied by high charge-discharge efficiencies of 91.4% and 84.1% at 150 ℃ and 200 ℃, respectively. These obtained performance in this work surpasses those of most previously reported mono-layered composite counterparts. This study provides a straightforward and effective strategy for designing high-temperature polymer dielectrics in advanced electrical and electronic systems, offering a new route for future applications and developments.

Keywords: Capacitor; Composite dielectrics; High temperature; Breakdown strength; Energy storage.

1. Introduction

Electrostatic capacitors have widespread applications in power pulse systems and power conditioners due to their ultrahigh power density and ultra- fast charging- discharging rate. Moreover, as an important branch, polymer-based film

dielectric capacitors play a pivotal role in home appliances, communication equipment, aerospace and military field owing to their outstanding performance, such as remarkable self-healing capability, high breakdown strength, exceptional stability, light weight and excellent processability [1-3]. Compared with alternative energy storage systems such as batteries, fuel cells and supercapacitors, dielectric capacitors based on polarization-depolarization are facing the critical challenge in effectively improving their energy density. Typically, the energy density (U_e) of dielectric capacitors hinges upon the dielectric constant (ε_r) and breakdown strength (E_b) [4]. Polymer dielectrics are particularly constrained by their low intrinsic polarization strength and ε_r. For example, biaxially oriented polypropylene (BOPP) exhibits a low ε_r (~2.1), resulting in a low U_e of approximately 2 J cm^{-3} [5]. However, insufficient energy density poses significant challenges regarding the large assembly volume and weight in current electrical and electronic applications, making it imperative to enhance the U_e of polymer dielectrics to support the continuous advancement of modern electronic devices towards miniaturization and high efficiency [6].

In addition, propelled by the thriving development in industries such as hybrid electric vehicles, aerospace engineering, and underground oil and gas exploration [7-10], there has been a substantial surge in demand for high-temperature capacitors (>150 °C). Regrettably, conventional polymer dielectrics fall short of meeting the elevated temperature requirements, primarily constrained by their inherently low glass transition temperatures (T_g). For instance, BOPP fails to maintain the long-term operational

stability when subjected to high electric fields exceeding 105 °C. In such condition, the conduction losses of BOPP would significantly escalate, impeding its efficient release of stored electrical energy. Instead, a considerable proportion of energy would be dissipated as wasted Joule heat, which could ultimately precipitate thermal runaway in the capacitor. Consequently, supplementary cooling systems have to be necessary, which largely augments both manufacturing expenses and power consumption within electronic power systems [11, 12]. In fact, an ideal high-temperature dielectric capacitor ought to feature not only a high U_e but also a charge-discharge efficiency (η) exceeding 90%, facilitating compact dimensions and minimizing heat dissipation of devices.

To address the urgent demand for high-temperature dielectric capacitors with high U_e and high η, researchers have extensively investigated the engineering plastics with high-T_g such as polyimide (PI) [13], polyetherimide (PEI) [14], polycarbonate (PC) [15], and polyaryl ether ketone (PAEK) [16]. These engineering plastics possess excellent thermal stability, good mechanical strength and outstanding insulation performance, making them as suitable candidates for high-temperature polymer dielectrics. However, compared to room temperature condition, both the electrical-insulation and U_e of these high-T_g polymers deteriorate significantly at the application scenario of elevated temperature and high electric field. In this case, a large number of charges could be injected into the dielectrics through the electrodes and accelerated by the electric field, continuously bombarding the macromolecular chains of polymer matrices. It results in the damage of the macromolecular chains, thereby affecting the functional performance

and stability of dielectrics. Moreover, the mutual collision of numerous carriers within the polymer dielectric generates a considerable amount of heat as well. As their inherent nature of poor thermal conductivity, such heat accumulation accelerates the damage and decomposition of the polymers, ultimately resulting in the thermal runaway of the polymer dielectric. For instance, when PI is subjected to 150 ℃ and under an electric field of 200 MV m^{-1}, its η is only 76%, with a U_e of merely 0.44 J cm^{-3}. This illustrates that a large proportion of stored energy is dissipated in the form of Joule heat. Moreover, at 250 ℃, the energy loss of PI almost reaches 100%, resulting in a complete loss of its practicality.[17] This loss mainly stems from the increase in leakage current density caused by Poole-Frenkel (*P-F*) and Schottky emission at elevated temperatures [17, 18]. Given that the deterioration of high-temperature performance poses a critical bottleneck, suppressing the injection and transmission of carriers to mitigate conduction losses at elevated temperatures has emerged as the primary principle in the design of polymer dielectrics.

To address this challenge, numerous strategies have been proposed to improve the high-temperature energy storage properties of polymer dielectrics. One approach involves the construction of inorganic insulating coating-layer on the surface of the high T_g polymer to inhibit the charge injection from the electrode. According to the charge transport mechanism, this method can effectively increase the barrier height at the interface between the electrode and the dielectric film, efficiently suppressing charge injection and reducing the conduction loss and leakage current density of the composites

at elevated temperatures [19-21]. However, on one hand, the inorganic coating-layer would increase the brittleness and hardness of the polymer dielectrics, which may impact its flexibility and self-healing property [22]. On the other hand, the mismatch in Young's modulus, huge difference in thermal expansion coefficients and weak adhesion between polymer film and inorganic coating-layer may lead to the peeling and delamination of inorganic coating, subsequently resulting in an increase in structural defects and conduction loss or even bringing about the failure of the polymer dielectrics [23].

Another strategy involves incorporating inorganic nanoparticles with wide bandgap and high breakdown strength (BN [24][17], Al_2O_3 [24], MgO [25], etc.) into polymer matrices, which significantly enhances the high-temperature energy storage capabilities of polymer dielectrics. This enhancement is achieved by altering the molecular energy levels between the inorganics and polymer matrices to construct traps at interfaces. These traps are advantageous for capturing charges within the composite system, thereby decreasing the number of carriers and limiting their transport, and reducing conduction losses in the composites. For instance, Fan et al. reported a high U_e of 3.7 J cm^{-3} and an ultra-high η of 90.1% at 150 °C and 500 MV m^{-1} were achieved by incorporating 1 vol% of Al_2O_3 into the PEI matrix [24]. Additionally, Wang et al. demonstrated that a U_e of 4.78 J cm^{-3} was achieved in MgO/PI composites filled with a small number of MgO nanosheets [25]. Although traps can be introduced into the polymer matrix by incorporating inorganic fillers, which typically have relatively low energy levels. This situation may hinder the effective capturing and scattering of charges, consequently

limiting the enhancement of energy storage performance and electrical stability at elevated temperatures. Based on this problem, in recent years, researchers have unveiled that the introduction of certain organic small-molecule semiconductors possessing high electron affinity, which can facilitate the establishment of deeper trap energy levels within the polymer matrix in contrast to inorganic fillers. This strategy enables an effective suppression of conduction losses and reduction of leakage current in composite dielectrics [26-28]. For example, Zhang et al. reported excellent U_e values of 5.1 J cm^{-3} and 3.2 J cm^{-3} with high η of 85-90% achieved from the 0.5 vol% 1,4,5,8-naphthalenetetracarboxylic dianhydride (NTCDA)/PEI at 150 °C and 200 °C, respectively [28]. Furthermore, Feng et al. effectively manipulated the concentration and position of traps formed by 3,9-bis(2-methylene-(3-(1,1-dicyanomethylene)-indanone))-5,5,11,11-tetrakis(4-hexylphenyl)-dithieno[2,3-d:2',3'-d']-sindaceno[1,2-b:5,6-b']-dithiophene (ITIC) in the PEI matrix via electrospinning techniques. The well-designed composite achieved a high U_e of 6.37 J cm^{-3} and a high η of 90% at 150 ℃ [27]. Although these molecule semiconductors can enhance the high-temperature energy storage properties of polymer dielectrics, they also encounter challenges that restrict their practical application range: (i) the necessary intricate synthesis and stringent processing control usually at the expense of higher production costs, thereby imposing significant constraints on their large-scale manufacturing and application [29]. (ii) the inherent sensitivity to high temperatures and humidity renders them vulnerable to be oxidized and decomposed, particularly for the

functional groups or unstable side chains, which may result in molecular loss or structural changes of molecule semiconductors, consequently affecting their functional performance under extreme conditions. (iii) the difficulty of the homogeneous dispersion and migration of organic small molecules also presents a significant challenge for the practical operation of dielectric capacitors [23].

Metal-organic frameworks (MOFs) are a class of crystalline compounds composed of metal ions and organic ligands. In recent years, researchers have made continuous progress in enhancing the high-temperature energy storage characteristics of composite dielectrics by employing various structural MOFs. This enhancement is mainly facilitated by the intrinsic features of MOFs, including high controllability, wide bandgap, excellent electrical-insulation property, and robust thermal stability. For instance, Li et al. constructed a multi-site bonding network within PEI matrix by using ZIF-8, where a U_e of 3.83 J cm^{-3} at 150 ℃ was achieved due to the dynamic stability of the multi-site bonding network at elevated temperatures [30]. Wang et al. prepared the mixed-metal MOFs (ZIF 8-67) by partially replacing metals in the nodes to widen the bandgap and reduce conductivity of the MOF, which is advantageous for capturing spatial charges in composites and preventing the growth of electric trees. The results demonstrated that ZIF 8-67/PEI obtained high U_e of 5.01 J cm^{-3} and 3.4 J cm^{-3} at 150 ℃ and 200 ℃, respectively [31]. This improvement demonstrates the enormous potential of MOFs in enhancing the high-temperature energy storage characteristics of composite dielectrics.

Unlike previously reported studies that focused on the inherent wide bandgap feature

of MOFs, we make use of the typical surface electron affinity of MOFs to regulate the migration of space charges through strong electrostatic attraction, thereby reducing the conduction losses of polymer dielectrics. In this work, by utilizing the high controllability of MOFs, a kind of typical ultrafine UIO-66 nanoparticles with the positively-charged surface and an ultrafine size of 12.9 nm was prepared using a solvent-free method. UiO-66 composed of zirconium-based metal nodes and the organic ligand 1,4-dicarboxybenzene (H_2BDC) is one of the most extensively used MOFs at present, exhibiting excellent stability in water, acidic/alkaline solutions, most organic solvents, and thermal conditions up to 500 °C. In comparison to conventional MOFs with hundreds of nanometers in size, the ultrafine UIO-66 nanoparticles synthesized in this study can further increase their bandgap width, which is conducive to the enhancement of its intrinsic insulating feature. Moreover, the positively-charged surface endows the UIO-66 nanoparticles with high electron affinity, which can trap injected and excited charges in the composites through strong electrostatic interaction, thereby suppressing the conduction loss of the composite dielectrics. Additionally, our previous finding has confirmed that diminishing the size of UIO-66 nanoparticles increases the Zeta potential due to a significant increase in specific surface area, which facilitates the formation of more active sites and enhances surface charge density [32], thereby benefiting the construction of charge traps with deeper energy levels in polymer dielectrics. Therefore, the positively-charged ultrafine UIO-66 nanoparticles were introduced into the PEI matrix by using the solution casting method to prepare the UIO-66/PEI composite

dielectrics. The research results demonstrate that ultrafine UIO-66 nanoparticles can enhance the overall ε_r of the composites by establishing strong heterogeneous interaction interfaces with the PEI matrix. Furthermore, UIO-66 with high electron affinity can introduce deeper traps in PEI matrix to effectively capture charges and inhibit carrier migration, which facilitates the reduction of conduction losses arising from Schottky and *P-F* emissions, thereby enhancing the E_b of the composites. Additionally, UIO-66 promotes the formation of a three-dimensional interpenetrating multi-site bonding network within composites, which positively affects the mechanical properties and further contributes to the improvement of E_b for the composites at elevated temperatures. Consequently, these combined effects give rise to the significantly improved energy storage property of UIO-66/PEI composites at elevated temperatures [33]. This work provides an effective mechanism for developing advanced polymer capacitors with excellent high-temperature energy storage characteristics.

2. Experimental Section

2.1 Materials

PEI particles (Ultem 1000) were provided by SABIC. N-Methyl-2-pyrrolidone (NMP) (>99%) and anhydrous ethanol (>99%) were supplied by Tianjin Kemiou Chemical Reagent Co., Ltd. Octahydrate zirconyl chloride (99.9%) was purchased from China National Pharmaceutical Group Chemical Reagent Co., Ltd. Hexahydrate ferric chloride (97%) was purchased from Tianjin Damao Chemical Reagent Factory. Phthalic acid

(H_2BDC) (>99%) was obtained from Shanghai Aladdin Bio-Chem Technology Co., Ltd. All chemical reagents are analytically pure and have not been further purified before use.

2.2 Synthesis of UIO-66 Nanoparticles

1.8 mmol of $ZrOCl_2 \cdot 8H_2O$ and 1.8 mmol of H_2BDC were mixed together and ground in an agate mortar for 15 min at room temperature. Subsequently, $FeCl_3 \cdot 6H_2O$ was added and the mixture was further ground for another 15 min. The resulting mixture was subsequently transferred to an autoclave and crystallized at 150 ℃ for 12 h. After the reaction was finished and cooled to room temperature, the resultant solid was washed with anhydrous ethanol and centrifuged. The precipitates were collected then mixed with 40 mL of anhydrous ethanol and sonicated for 90 min through an ultrasonic cleaner. The supernatant was collected and allowed to settle naturally. The precipitated product was then added to deionized water and frozen at -18 ℃ for 12 h. Finally, the frozen sample was transferred to a vacuum freeze dryer and freeze-dried for 72 h to obtain well-dispersed UIO-66 nanoparticles.

2.3 Preparation of UIO-66/PEI Composites

The UIO-66/PEI composites were prepared by using the typical solution casting method. Initially, different weight ratios of UIO-66 nanoparticles (0 wt%, 0.25 wt%, 0.5 wt%, 0.75 wt%, 1.0 wt%, 1.25 wt%) were precisely weighed and dispersed into NMP solution. After 30 min of ultrasonication, well-dispersed UIO-66/NMP suspensions were obtained. Subsequently, PEI particles were added to the UIO-66/NMP suspension and vigorous magnetic stirring was conducted at 70 ℃ for 8 h to obtain a homogeneous

mixture. The mixture was then degassed in a vacuum chamber to remove air bubbles. Next, the mixture was cast onto a clean quartz plate at a speed of 50 mm s^{-1} by using a film applicator. The casted mixture was then placed in a blast drying oven at 80 ℃ for 12 h to evaporate most of the solvent. Finally, it was heated to 200 ℃ and maintained for 6 h to eliminate any residual solvent to obtain the UIO-66/PEI composites.

2.4 Characterization

The morphologies of UIO-66 nanoparticles were characterized by a transmission electron microscopy (TEM, Tecnai G2 F20 S-TWIN, FEI, Ohio, USA). The cross- section images of UIO-66/PEI composites were characterized by a scanning electron microscopy (SEM, Zeiss Sigma 300, Thermo Scientific, USA) coupled with energy-dispersive X-ray spectroscopy (Thermo Scientific UltraDry, USA). The samples needed to be cryogenically fractured in liquid nitrogen before the composites were characterized by SEM. The crystal structure of UIO-66 nanoparticles was investigated by employing a X-ray diffraction (XRD) analysis (Bruker D8 Advance) within the 2θ range of 5° to 35° using Cu-Kα radiation (λ=1.54 Å). The elemental composition of UIO-66 nanoparticles was analyzed by X-ray photoelectron spectroscopy (XPS, PHI-5400, ULVCAPHI, Japan) using Al Kα as the X-ray source. Zeta potential measurement of UIO-66 was measured using a Zeta potential analyzer. Dielectric constant and loss testing were performed using a wide-frequency impedance analyzer (Novocontrol Concept 40, Germany) over a broad temperature range of 25-200 ℃. Thermal stimulated depolarization current (TSDC) measurements of the composites were also carried out

using the wide-frequency impedance analyzer. The breakdown strength of the composites was tested under conditions of a voltage ramp rate of 200 V s^{-1} and a current limit of 5 mA using a high-voltage source (CS9920B, Nanjing, China). Unipolar electric displacement-electric field (*D*-*E*) hysteresis loops at the frequency of 50 Hz within the temperature range of 25-200 ℃ were collected using a ferroelectric analyzer (Radiant Technologies Precision Premier II, USA) with a maximum voltage of 10 kV.

3. Results and discussion

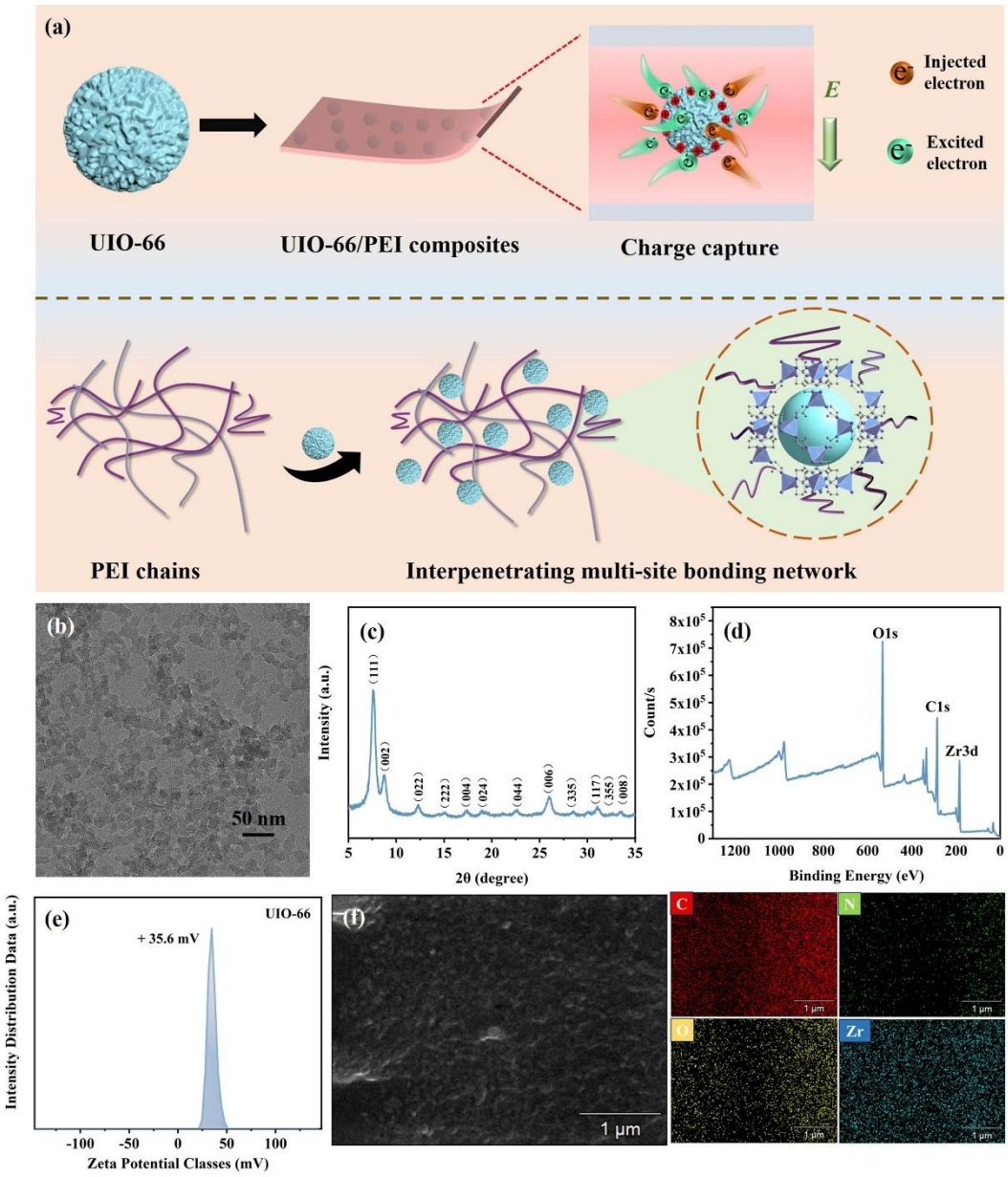

Fig. 1. (a) Schematic illustration of charge capture by UIO-66 nanoparticles and the interpenetrating bonding network between PEI chains and UIO-66 nanoparticles; (b) TEM image; (c) XRD pattern; (d) XPS characterization and (e) The Zeta potential of as-synthesized UIO-66 nanoparticles; (f) Cross-sectional SEM image of the 0.5 wt% UIO-66/PEI composite. Corresponding EDS mapping of C, N, O and Zr elements.

Fig. 1a depicts the schematic illustration of charge capture by UIO-66 nanoparticles

and the interpenetrating bonding network between PEI chains and UIO-66 nanoparticles. As depicted in the TEM image of Fig. 1b, the UIO-66 nanoparticles prepared by the solvent-free method exhibit an ellipsoidal shape, excellent dispersion among the nanoparticles with no noticeable agglomeration, and an average diameter of approximately 12.9 ± 1.5 nm (Fig. S1). As shown in Fig. 1c, the diffraction peaks observed at 7.4° and 8.5° in the XRD pattern correspond to the characteristic peaks of standard UIO-66, specifically the (111) and (002) crystal planes in the face-centered cubic structure of UIO-66 crystals [32, 34]. Fig. 1d illustrates the XPS characterization of UIO-66, indicating that the synthesized UIO-66 mainly consists of C, O, and Zr elements. Zeta potential characterization was conducted on UIO-66 nanoparticles to investigate their surface charge features. As shown in Fig. 1e, the average potential of UIO-66 is +35.6 mV, suggesting its positively-charged surface possesses strong cationic surface characteristics [35], which enable it to engage in strong electrostatic interactions with free charges in the surrounding environment, effectively capturing the injected and excited charges in composite dielectrics. Fig. 1f and Fig. S2 display the cross-sectional SEM image of the 0.5 wt% UIO-66/PEI composite, revealing a relatively flat and dense morphology without obvious cracks or voids, affirming that the prepared composite thin film (thickness ~ 6 μm) possesses high quality and good compatibility between UIO-66 and PEI matrix. Furthermore, EDS mapping demonstrates the uniform dispersion of the distinctive Zr element of UIO-66, suggesting the good dispersion of UIO-66 in the PEI matrix.

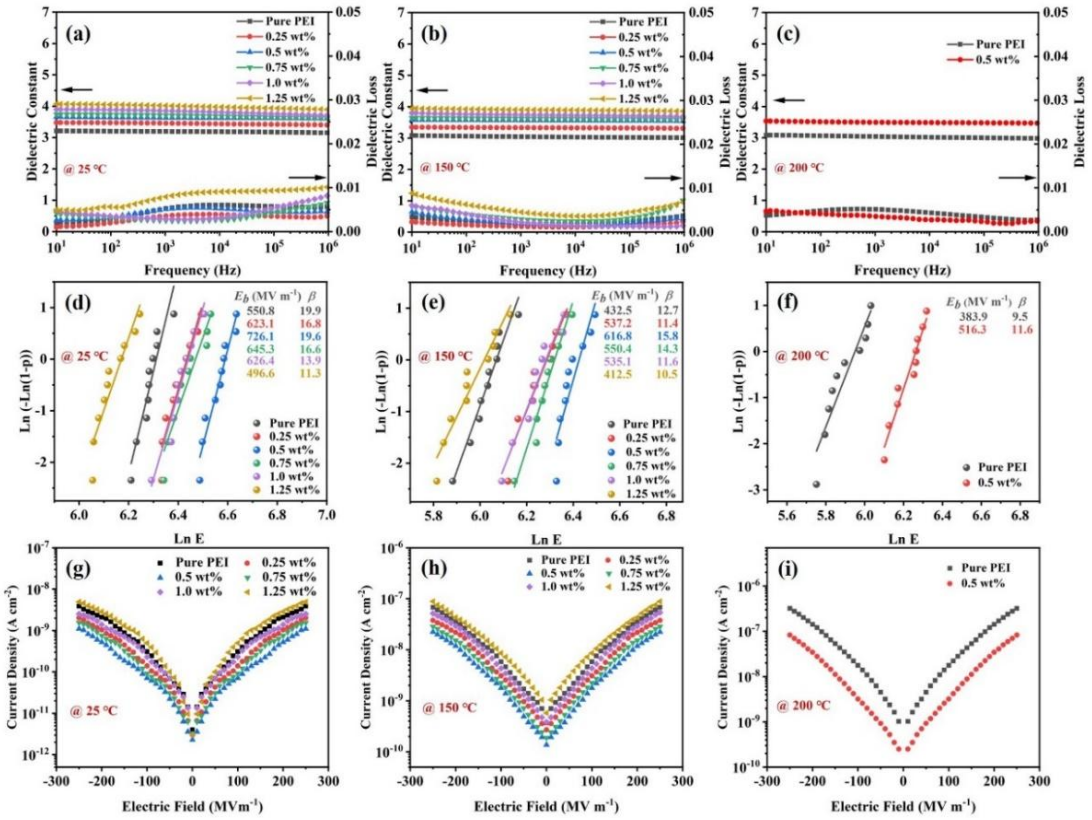

Fig. 2. Frequency-dependent dielectric constant and dielectric loss of pure PEI and UIO-66/PEI composites at (a) 25 ℃; (b) 150 ℃ and (c) 200 ℃; Weibull breakdown distribution of PEI and UIO-66/PEI composites at (d) 25 ℃; (e) 150 °C and (f) 200 °C; leakage current density as a function of electric field for PEI and UIO-66/PEI at (g) 25 ℃; (h) 150 ℃ and (i) 200 ℃.

The frequency-dependent behaviors of the dielectric constant (ε_r) and dielectric loss ($tan\ \delta$) of UIO-66/PEI composites at different temperatures are depicted in Fig. 2a-c and Fig. S3-4. As illustrated in Fig. 2a, it is evident that UIO-66/PEI composites exhibit remarkable frequency-dependent stability across the testing frequency range from 10 Hz to 10^6 Hz, with negligible fluctuation in ε_r. Moreover, the ε_r of UIO-66/PEI composites increases with increasing UIO-66 filling content at 25 ℃. Specifically, the ε_r escalates from 3.2 for pure PEI to 4.05 for the composite containing 1.25 wt% UIO-66

nanoparticles at 100 Hz. The significant increase in ε_r at low concentrations is primarily attributed to the permanent dipole polarization induced by UIO-66 nanoparticles. Additionally, the disparity in electrical properties between UIO-66 and PEI matrix gives rise to varying carrier mobility, facilitating the accumulation of free charges at the interface, thereby enhancing the interfacial polarization within the composites [36]. Moreover, UIO-66 with strong cationic surface feature can engage in significant electrostatic interaction with the surrounding charges, which significantly enhances the polarization effect of the composite and thereby increases its ε_r. Furthermore, the ultrafine UIO-66 nanoparticles possess the inherent porous structure and an exceptionally large specific surface area, which is beneficial to the formation of strongly interacting heterogeneous interfaces with PEI matrix. In fact, this enhanced interfacial interaction plays an important role in improving the overall ε_r of the composites. Meanwhile, the *tan* δ of all composites remains below 0.01, demonstrating that the composites exhibit low leakage current and low energy loss. On one hand, the low *tan* δ is attributed to the rigid framework of PEI, which is less susceptible to polarization under external electric fields, thereby facilitating the reduction in energy dissipation. On the other hand, ultrafine UIO-66 nanoparticles can construct a special multi-site bonding network with PEI matrix [30]. In comparison to pure PEI, the organic macromolecular chains can be firmly bonded with UIO-66 nanoparticles in the composites, enabling fewer macromolecular chains and side groups to respond to the electric field in time, thereby minimizing the losses caused by dipole orientation polarization. As shown in Fig. 2b-c and Fig. S4a-b,

the frequency dependence of ε_r and *tan* δ for the composite dielectrics at 100 °C, 150 °C, and 200 °C exhibits a similar trend to those obtained at 25 °C. Additionally, Fig. S4c-d illustrates the temperature dependence of ε_r and *tan* δ of UIO-66/PEI composites at 100 Hz. It is noteworthy that the ε_r of UIO-66/PEI demonstrates a slight decrease as the temperature escalates from 25 ℃ to 200 ℃. This decrease is mainly attributed to that the alignment of intrinsic dipole moments can be promoted by the external electric field while disrupted by thermal excitation. Consequently, the molecules within UIO-66/PEI composites undergo vigorous thermal motion with rising temperature, impeding the orientation of polar phthalimide molecules in PEI along the direction of the electric field, thereby diminishing the overall dipole polarization level in the UIO-66/PEI composite system [1]. Meanwhile, the *tan* δ of UIO-66/PEI composites exhibits a slight improvement with the elevated temperature, primarily due to the escalation of conduction losses caused by thermal excitation. Nevertheless, the *tan* δ of UIO-66/PEI composites remains at a low level (< 0.01). Therefore, the minor fluctuations in both ε_r and *tan* δ of UIO-66/PEI composites with elevated temperature suggest their excellent thermal stability in dielectric performance, implying promising energy storage capabilities at elevated temperatures [37].

Comprehensive electrical characterization was conducted to elucidate the pivotal role of ultrafine UIO-66 nanoparticles with high electron affinity in achieving the excellent electrical performance of UIO-66/PEI composites. Fig. 2d-f and Fig. S5 depict the Weibull distribution of E_b and the β values for pure PEI and UIO-66/PEI composites

measured at temperatures ranging from 25 ℃ to 200 ℃. The E_b values of the UIO-66/PEI composites exhibit a trend of initially increasing and subsequently decreasing with increasing UIO-66 filling content at all testing temperatures. Remarkably, the 0.5 wt% UIO-66/PEI composite achieves the maximum E_b of 726.1 MV m^{-1}, which is improved by 31.8% compared to that of pure PEI (~550.8 MV m^{-1}) at 25 ℃. However, the E_b of all samples decreases with increasing temperature, which can be attributed to the exponential growth of conduction loss, primarily dominated by Schottky injection and *P-F* emission at elevated temperatures, leading to a notable increase in leakage current [38]. As shown in Fig. S5a, the E_b of pure PEI decreases to 432.5 MV m^{-1} and 389.3 MV m^{-1} at 150 ℃ and 200 ℃, respectively. Notably, the 0.5 wt% UIO-66/PEI composite achieves the improved E_b values of 616.8 MV m^{-1} and 516.3 MV m^{-1} at the same temperatures, respectively (Fig. S5b), which increased by 42.6% and 32.6% compared to pure PEI. Meanwhile, the 0.5 wt% UIO-66/PEI composite exhibits the highest β value at all testing temperatures, indicating that the obtained excellent performance also contributed by its good structure stability. The significant enhancement in E_b of UIO-66/PEI composites can be explained in several aspects: (i) ultrafine UIO-66 nanoparticles are uniformly dispersed in the PEI matrix without significant agglomeration, which weakens the inhomogeneity of the local electric field inside the composites; (ii) According to the electromechanical breakdown theory, polymer dielectrics are susceptible to electro-mechanical breakdown at elevated temperatures since the Young's modulus (Y) decreases with increasing temperature. It is seen from Fig.

S6 that the addition of UIO-66 nanoparticles can significantly increase the *Y* of the composites, which is partly attributed to the rigid characteristics of UIO-66. (iii) UIO-66 can serve as molecular nodes to construct a multi-point bonding network within the PEI matrix, thereby limiting the movement of PEI macromolecular chains and improving the E_b of composites [30]. Consequently, the enhancement in *Y* of UIO-66/PEI composite reduces the risk of breakdown.

When the filling content of UIO-66 reaches 1.25 wt%, the E_b of the composites decreases to 496.6 MV m^{-1} and 412.5 MV m^{-1} at 25 ℃ and 150 ℃, respectively, both of which are even lower than those of pure PEI. This decline may be attributed to the formation of agglomerates of excessive UIO-66 in PEI matrix, resulting in the formation of defects at the fillers-matrix interface. The trend in E_b of the composites at different temperatures correlates closely with the distribution of leakage current density (*J*) illustrated in Fig. 2g-i. The *J* of UIO-66/PEI composites initially decreases and then increases with growing UIO-66 content under a constant electric field. Additionally, a reduction in *J* is observed for the composites when incorporated with less than 1.25 wt% UIO-66 nanoparticles. Notably, the 0.5 wt% UIO-66/PEI composite demonstrates the lowest *J* under the condition of identical electric field and temperatures. The reduction in *J* indicates that ultrafine UIO-66 nanoparticles with high electron affinity can effectively suppress the injection and transport of charges in the composites.

In fact, ultrafine UIO-66 nanoparticles with high electron affinity can play a crucial role in regulating the E_b of the composites. Finite element analysis was employed to further reveal the impact of positively-charged ultrafine UIO-66 nanoparticles on the redistribution of local electric field. Compared with pure PEI (Fig. S7a), the addition of UIO-66 can significantly varies the local electric field distribution in composites (Fig.

S7b-c). The migration of space charge in different interfacial regions of UIO-66/PEI composites is affected by varying electric field-driven force, which is attributed to the weakening (blue regions) or strengthening (orange-red areas) of the local electric field strength. As shown in Fig. S7b, the large areas of low localized electric field connect with each other (blue areas) to form an in-plane shielding layer that is perpendicular to the direction of the electric field when an appropriate content of ultrafine UIO-66 nanoparticles is filled. When charges migrate to this region, their migration rate decreases. It is beneficial to mitigating both conduction loss and leakage current in the composites, consequently enhancing the overall E_b. However, as the UIO-66 filling content further increases (>1.0 wt%) (Fig. S7c), the initially established in-plane shielding layer is gradually disrupted due to the partially overlapping of regions with high localized electric fields (orange-red areas). When charges migrate to this region, a significant acceleration effect on the movement of charges is generated, promoting the growth of the electric tree and negatively affecting the maintenance in E_b of the composite.

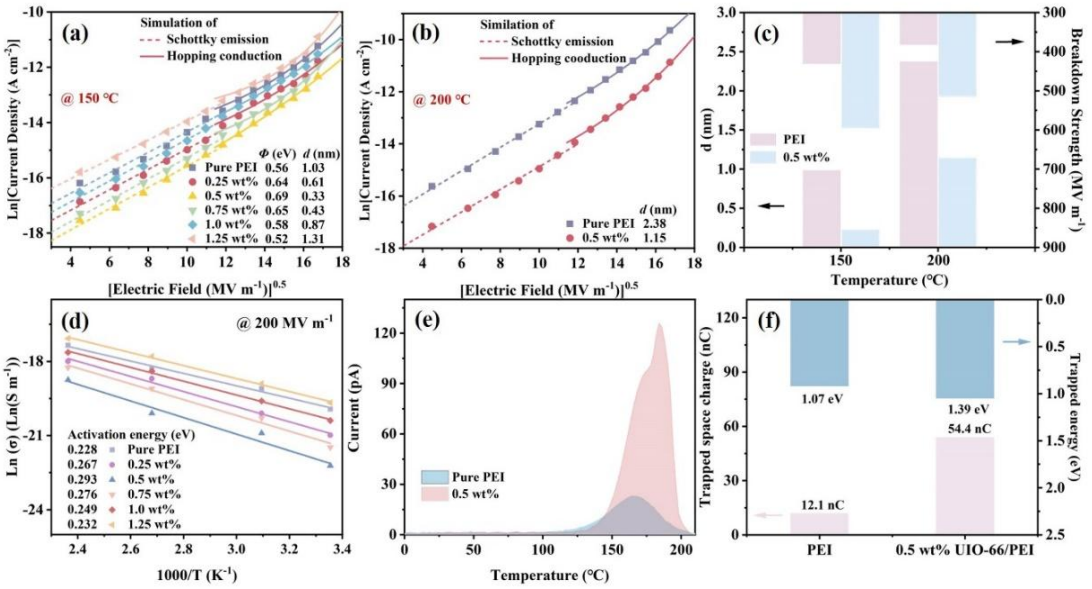

Fig. 3. Leakage current density of PEI and UIO-66/PEI composites as a function of electric field at (a) 150 ℃ and (b) 200 ℃; (c) Hopping distance and breakdown strength of PEI and the 0.5 wt%

UIO-66/PEI composite at different temperatures; (d) Temperature-dependent electrical conductivity at 200 MV m^{-1}; (e) TSDC curves of PEI and the 0.5 wt% UIO-66/PEI composite; (f) Trapped space charge and trap energy level of PEI and the 0.5 wt% UIO-66/PEI composite.

To elucidate the breakdown mechanism of UIO-66/PEI composites at elevated temperatures, an in-depth investigation into their internal charge conduction is indispensable. The *J* values of both pure PEI and 0.5 wt% UIO-66/PEI composite at different temperatures under an applied electric field of 250 MV m^{-1} are illustrated in Fig. S8, which exhibits an increasing trend with rising temperature. However, it is noteworthy that the *J* value of the 0.5 wt% UIO-66/PEI composite is considerably lower than that of pure PEI, regardless of at ambient or elevated temperatures. Specifically, at 150 ℃, the *J* of the 0.5 wt% UIO-66/PEI composite is 2.25×10^{-8} A cm^{-2}, which is only 33% of that of pure PEI (6.80×10^{-8} A cm^{-2}). At 200 ℃, the *J* of the 0.5 wt% UIO-66/PEI composite increases to 8.26×10^{-8} A cm^{-2}, representing only 25.8% of that of pure PEI (3.21×10^{-7} A cm^{-2}) as well. In fact, the *J* exhibits an exponential growth trend with increasing electric field at elevated temperatures, primarily due to the Schottky and *P-F* emission in the composites [38].

To further elucidate the influencing mechanism of Schottky and *P-F* conduction in conduction losses at elevated temperatures for both pure PEI and UIO-66/PEI composites, the Schottky emission model for the low electric field region and the hopping conduction model for the high electric field region were separately employed to analyze the *J* as a function of the applied electric field (Fig. 3a-b). The fitted curves in the figures exhibit a good coincidence with the experimental data, suggesting that the internal charge conduction in both pure PEI and UIO-66/PEI composites conforms to these conduction models at elevated temperatures. Furthermore, the fitting of *J* versus electric field data at elevated temperatures reveals that the conduction mechanism in composite dielectrics

transitions from charge injection-controlled Schottky emission to transport-limited hopping conduction with increasing the electric field. Such transition could be attributed to the saturation of charge trapping near the electrode/dielectric interface [29]. According to the results from the Schottky emission fitting model, the barrier heights (Φ) of pure PEI and the 0.5 wt% UIO-66/PEI composite are 0.56 eV and 0.69 eV, respectively. The enhanced Φ values suggest that introducing ultrafine UIO-66 can effectively mitigate the electrode-limited conduction loss in the composites. In addition, the ultrafine UIO-66 with high electron affinity can serve as the trap site to capture the injected charges. The hopping distance (d) correlates with the distance among the neighboring trapping sites and the depth of charge traps inside the composite dielectrics. As demonstrated in Fig. S9a, the d value of UIO-66/PEI composite at 150 °C exhibits a trend of initially decreasing and then increasing with growing UIO-66 content, which correlates with the behavior observed in the J. Specifically, the d values of pure PEI and the 0.5 wt% UIO-66/PEI composite are 1.33 nm and 0.33 nm at 150 °C, respectively, which increase to 2.38 nm and 1.15 nm at 200 °C, respectively. (Fig. S9a-b). Moreover, as illustrated in Fig. 3c, it is noteworthy that the d value of the 0.5 wt% UIO-66/PEI composite is significantly lower than that of pure PEI at elevated temperatures. Consequently, incorporating ultrafine UIO-66 nanoparticles with high electron affinity into PEI can be advantageous for increasing of the strong heterogeneous interaction interfaces, thereby effectively constructing the greater number of trap sites and deeper traps within the composite dielectrics. These additional deep traps are beneficial to enhancing the efficiency of trapping charge, making it challenging for charges to escape from them. Therefore, the conduction loss caused by Schottky and *P-F* emission is effectively mitigated by the ultrafine UIO-66 with high electron affinity at elevated temperatures, which suppresses leakage current density and enhances E_b of UIO-66/PEI composites.

Furthermore, the activation energy associated with charge trapping is determined from the temperature-dependent conductivity of PEI and UIO-66/PEI composites and analyzed using the Arrhenius formula, as shown in Fig. 3d. The highest thermal activation energy (0.293 eV) is demonstrated by the 0.5 wt% UIO-66/PEI composite, which surpasses that of pure PEI (0.228 eV). It is further indicated that the deepest charge trapping energy level can be introduced by incorporating 0.5 wt% UIO-66 nanoparticles, effectively capturing high-energy electrons and consequently inhibiting carrier migration within the PEI matrix. Therefore, it is implied that the trap depth of the composites may be more effectively increased by the presence of ultrafine UIO-66 nanoparticles [38].

To evaluate the energy levels of interfacial trap and gain insight into the relationship between trap depth and electron conduction behavior, TSDC characterization was conducted on pure PEI and the 0.5 wt% UIO-66/PEI composite. As depicted in Fig. 3e, a depolarization current peak of approximately 23 pA at around 164 °C is observed on the TSDC curve of pure PEI, correlating with the number of space charges. However, the depolarization current peak of the 0.5 wt% UIO-66/PEI composite appears around 184 °C with a corresponding current density of 123 pA. This shift of depolarization current peak towards higher temperatures and the increase in peak intensity collectively indicate that the ultrafine UIO-66 nanoparticles with high electron affinity can lead to the formation of additional new deeper trap levels and increased trap density, which facilitates the efficiency of trapping charge. The trapping energy levels (A_{TSDC}) and the quantity (Q_{TSDC}) of trapped charges can be derived from the TSDC curve, according to the half-width method [39, 40]. As illustrated in Fig. 3f, the A_{TSDC} and Q_{TSDC} increase from 1.07 eV and 12.1 nC for pure PEI to 1.39 eV and 54.4 nC for 0.5 wt% UIO-66/PEI composite, respectively. These enhancements signify that the 0.5 wt% UIO-66/PEI composite possesses deeper trap levels and a greater capacity to capture charges

compared to pure PEI. The activation of these deep traps effectively suppresses the escape of charge, thereby the conduction losses in the composites can be mitigated at elevated temperatures and high electric fields.

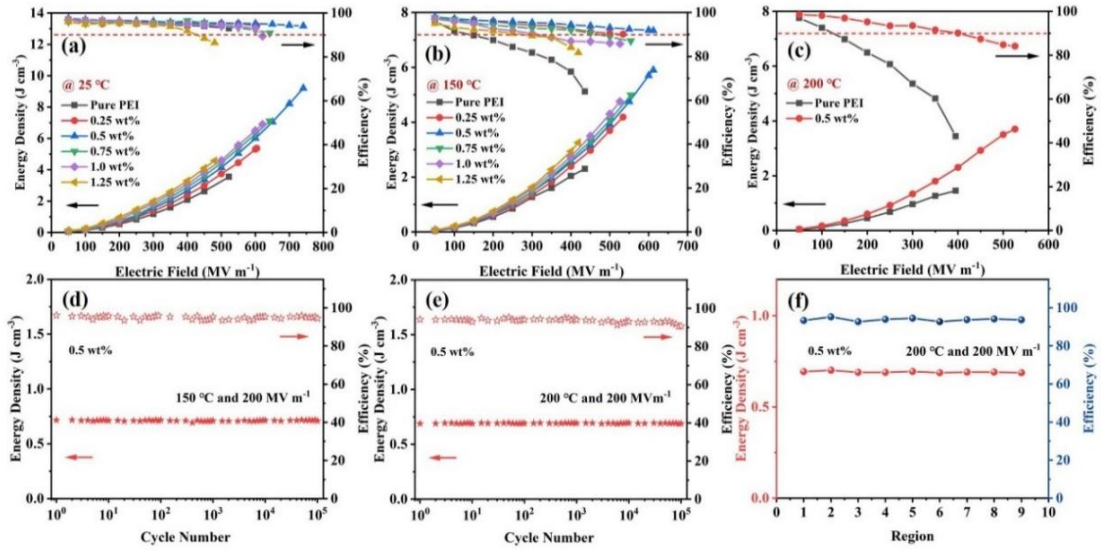

Fig. 4. Energy densities and charge-discharge efficiencies as a function of electric field for PEI and the UIO-66/PEI composites at (a) 25 ℃; (b) 150 ℃ and (c) 200 ℃; Energy densities and charge-discharge efficiencies of the 0.5 wt% UIO-66/PEI composite with cycle number under 200 MV m^{-1} at (d)150 ℃ and (e)200 °C; (f) Energy density and charge-discharge efficiencies achieved in different regions of the 0.5 wt% UIO-66/PEI composite film at 200 °C and 200 MV m^{-1}.

Unipolar *D-E* loops were utilized to characterize the polarization behavior of pure PEI and the UIO-66/PEI composites at 25 °C, 150 °C and 200 °C, as illustrated in Fig. S10-16. The U_e and η can be obtained by integrating the effective area of the *D-E* loops (Fig. 4a-c). As depicted in Fig. S10, both pure PEI and UIO-66/PEI composites at 25 °C exhibit typical characteristics of linear dielectrics [39]. Furthermore, the significantly enhanced displacement is exhibited by the UIO-66/PEI composites compared to pure PEI at the same electric fields (Fig. S11), which is consistent with the increase of their ε_r. It is noteworthy that the U_e of all UIO-66/PEI composites surpasses that of pure PEI due to the synergistic enhancement in both ε_r and E_b in the composites. Moreover, both the

maximum displacement (D_{max}) and U_e of the composites exhibit a trend of initially increasing and then decreasing with growing UIO-66 content. Notably, the maximum U_e is obtained from the 0.5 wt% UIO-66/PEI composite. Due to its low intrinsic polarization, pure PEI exhibits the maximum U_e of as low as 3.6 J cm^{-3} and η of 93% at 550.8 MV m^{-1} (Fig. 4a). However, the maximum U_e of 9.2 J cm^{-3} (under 726.1 MV m^{-1}) is obtained from the 0.5 wt% UIO-66/PEI composite, which is 156% higher than that of pure PEI counterpart. Simultaneously, the 0.5 wt% UIO-66/PEI composite achieves an exceptionally high η value of 94%. Therefore, the introduction of ultrafine UIO-66 nanoparticles with high electron affinity is advantageous in reducing conduction losses caused by leakage currents, thereby increasing the η value of the composites.

Fig. S12-13 depicts the *D-E* loops of pure PEI and UIO-66/PEI composites at elevated temperatures. While pure PEI demonstrates typical characteristics of a linear dielectric with nearly linear *D-E* loops at room temperature, a significantly increased residual polarization (D_r) is observed due to the sharp increase in leakage current at elevated temperatures. Compared to pure PEI, the introduction of UIO-66 leads to thinner *D-E* loops achieved in the composites, accompanied by a notable reduction in D_r and a significant increase in D_{max} (Fig. S14-15). As depicted in Fig. 4b, pure PEI at 150 ℃ obtains the maximum U_e of only 2.3 J cm^{-3} with a η of 64% at 432.5 MV m^{-1}. The 0.5 wt% UIO-66/PEI composite delivers a significantly higher maximum U_e of 5.9 J cm^{-3} and a η of 91% at 616.8 MV m^{-1}, which represents the impressive enhancements of 157% in U_e and 43% in η compared to pure PEI. Furthermore, with η around 90%, the U_e for the 0.5 wt% UIO-66/PEI composite surges by an astonishing 1743%, from 0.32 J cm^{-3} for pure PEI to 5.9 J cm^{-3}, highlighting the substantial performance advantages of the composite. The obtained sharp deterioration in energy storage performance of pure PEI is mainly attributed to the exponential growth of the conduction loss as the temperature rises from

150 °C to 200 °C (Fig. 4c). At 200 °C, pure PEI achieves the maximum U_e of only 1.45 J cm^{-3} with a η of only 43% at 389.3 MV m^{-1}. Conversely, the maximum U_e for the 0.5 wt% UIO-66/PEI composite is still as high as 3.7 J cm^{-3} with a relatively high η of 84.1%, representing a 156% increase in maximum U_e and a 96% increase in η compared to pure PEI. As for the condition of 200 °C and η around 90%, the maximum U_e is increased by 1382% from 0.17 J cm^{-3} at 120 MV m^{-1} for pure PEI to 2.52 J cm^{-3} at 516.2 MV m^{-1} for the 0.5 wt% UIO-66/PEI composite.

The 0.5 wt% UIO-66/PEI composite demonstrates excellent energy storage performance at elevated temperatures. To investigate the temperature stability of its energy storage properties, the *D-E* loops were measured from 25 °C to 200 °C. As shown in Fig. S16-17, it is observed that under a constant electric field below 400 MV m^{-1}, the U_e and η values of the 0.5 wt% UIO-66/PEI composite exhibit minimal variation with increasing temperature. However, under higher electric fields (>400 MV m^{-1}), the elevated temperature results in a decrease in both U_e and η values of the 0.5 wt% UIO-66/PEI composite. This reduction is due to that the violent molecular movement induced by elevated temperatures could hinder the orientation of polar molecules, thereby diminishing the overall dipole polarization of the composite [1]. Additionally, this behavior is also related to the increased energy loss due to Joule heating generated inside the composites at elevated temperatures [41].

It is well known that the cycling stability of film capacitors at elevated temperatures is crucial for practical applications. In order to mimic the electrical fatigue reliability of composite dielectrics under operating conditions in electric vehicles [11, 42], cycling tests were conducted on the 0.5 wt% UIO-66/PEI composite under 200 MV m^{-1}, at 150 °C and 200 °C. As shown in Fig. 4d-e, both U_e and η remain stable and no sign of performance degradation can be observed over 100000 charge-discharge cycles at

elevated temperatures. This result indicates that the 0.5 wt% UIO-66/PEI composite exhibits excellent thermal stability and reliability, highlighting its great potential for applications in high-temperature capacitors. In addition, in order to verify the uniformity and quality of the composite dielectric film, samples from various regions of the 0.5 wt% UIO-66/PEI composite were selected to measure the U_e and η at 200 °C and 200 MV m^{-1} (Fig. 4f). It is seen that the U_e and η values of 0.5 wt% UIO-66/PEI composite from nine different regions remain stable, which demonstrates the high uniformity of the composite film. The uniformity of UIO-66/PEI composite plays a crucial role in improving the consistency of electrical performance, mitigating premature failures caused by local performance variations, and consequently extending its service life. Specifically, the incorporation of ultrafine UIO-66 is conducive to stabilize the electrical properties and thermal stability, making the composite more reliable under varying operational conditions.

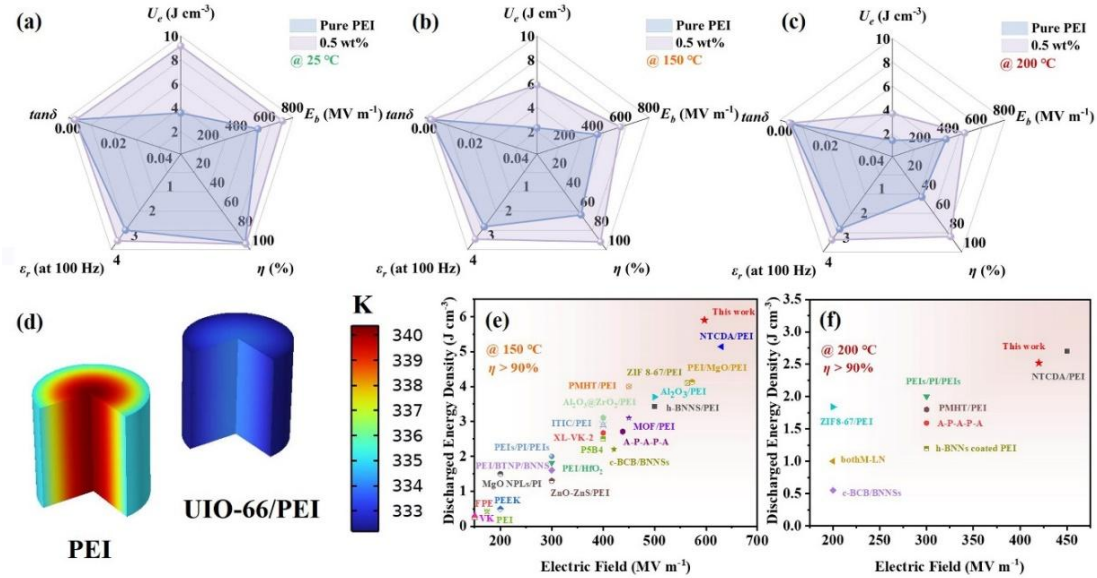

Fig. 5. Dielectric and capacitive parameters of PEI and the 0.5 wt% UIO-66/PEI composite measured at (a) 25 ℃; (b) 150 ℃ and (c) 200 ℃; (d) Finite-element analysis of the variation and distribution of temperature inner the film capacitor composed of PEI and the 0.5 wt% UIO-66/PEI composite at 200

MV m^{-1} with an ambient temperature of 200 ℃; Comparison of the discharged energy density with an efficiency around 90% achieved in this work with those of previously reported polymer and their composites at (e) 150 ℃ and (f) 200 ℃.

The practical feasibility and potential applications of composite dielectrics hinge significantly on their overall properties. Consequently, typical radar charts are employed to compare the multiple performance parameters (ε_r, *tan* δ, E_b, U_e, and η) of pure PEI and the 0.5 wt% UIO-66/PEI composite at different temperatures, in order to clearly assess the comprehensive contribution of ultrafine UIO-66 to composites. In a radar chart, the larger area signifies superior comprehensive performance of dielectrics. As illustrated in Fig. 5a-c, compared to that of pure PEI, the significantly larger area of the 0.5 wt% UIO-66/PEI composite clearly indicates its superior comprehensive performance. It is noteworthy that the area-ratio between pure PEI and the 0.5 wt% UIO-66/PEI composite in the radar chart decreases with increasing temperature, specifically dropping from 66.6% at 25 ℃ to 59.7% at 150 ℃ and further to 55.1% at 200 ℃. This trend reflects that due to the elevated temperature can induce a significantly higher conduction loss in pure PEI, resulting in a more pronounced deterioration in all parameters such as E_b, U_e and η of pure PEI. On the contrary, at same temperatures, the 0.5 wt% UIO-66/PEI composite still maintains larger areas in the radar chart, highlighting its significant advantages over pure PEI, further validating the dominant role of ultrafine UIO-66 nanoparticles with high electron affinity in enhancing the energy storage performances of PEI.

The finite-element analysis is employed to simulate the steady-state temperature distribution of wound film capacitor composed of pure PEI and the 0.5 wt% UIO-66/PEI composite under an applied electric field of 200 MV m^{-1} and at an ambient temperature of 200 ℃. As depicted in Fig. 5d, a significant temperature enhancement can be observed inside PEI-capacitor and the maximum temperature reaches approximately 340 K, which

exceeds that observed at the corresponding position in the composite-capacitor (~334 K). Moreover, the temperature difference between the interior and exterior of the PEI-capacitor is approximately 6 ℃, whereas that of the composite-capacitor is about 2 ℃. This discrepancy is mainly attributed to that the substantial conduction loss ultimately converts to the undesirable Joule heat that accumulated in PEI-capacitor. In contrast, the ultrafine UIO-66 can construct deep traps that inhibit charge injection and transport in the composite-capacitor, which reduces the leakage current density of the capacitors and consequently lowering the heat generation power.

In a word, both the U_e and η of PEI at elevated temperatures can be effectively improved by utilizing ultrafine UIO-66 nanoparticles with high electron affinity. The U_e of the UIO-66/PEI composite with a η of ~90% at 150 ℃ (5.9 J cm^{-3}) and 200 ℃ (2.52 J cm^{-3}) achieved in this work outperform those of most of the previously reported polymer and polymer-based composite dielectrics (Fig. 5e-f) [11, 13, 17,19, 24, 25, 27, 28, 30, 31, 43-53], with the full name and corresponding references provided in Tables S2-3. Due to its unique electronegative feature, the ultrafine UIO-66 nanoparticles can serve as effective agents to not only modulate the charge migration through strong electrostatic interaction buy also reduce the leakage currents caused by *P-F* and Schottky emissions. Therefore, outstanding U_e and η values in this study are obtained from the UIO-66/PEI composite dielectric, which makes it highly promising for fabricating composite dielectrics intended for harsh environments applications.

4. Conclusion

In summary, ultrafine UIO-66 nanoparticles with an ultrafine size of 12.9 nm were synthesized using a solvent-free method. A series of UIO-66/PEI composites with

varying weight fractions were prepared by using the solution casting method. Due to its unique high electron affinity, the deep trap levels can be successfully constructed by judiciously incorporating these ultrafine UIO-66 nanoparticles into PEI matrix. Consequently, the charge migration in UIO-66/PEI composites can be regulated by the strong electrostatic interaction generated by ultrafine positively-charged UIO-66 nanoparticles, reducing the overall conduction loss caused by Schottky and *P-F* emission at elevated temperatures, thereby significantly improving the comprehensive energy storage properties such as E_b, U_e and η of the composite dielectrics. Specifically, at 150 °C, the 0.5 wt% UIO-66/PEI composite achieves an ultra-high U_e of 5.9 J cm^{-3} with a η of 91.4%. Even at 200 °C, the 0.5 wt% UIO-66/PEI composite still maintains an ultra-high U_e of 3.7 J cm^{-3} with a η of 84.1%, and achieves a U_e of 2.52 J cm^{-3} with a η around 90%. These outstanding characteristics are very attractive for high-temperature capacitors and the straightforward synthesis process offers a novel approach for developing composite dielectrics with high U_e and η in extreme environmental conditions.

CRediT authorship contribution statement

Na Zhang: Idea, Experiment, Data analysis, Writing-Original Draft. **Hang Zhao:** Idea, Investigation, Supervision, Funding acquisition, Project administration, Writing-Revising and Editing. **Chuying Zhang**: Visualizations. **Haotong Guo**: Data analysis. **Zhi-Min Dang**: Writing-Revising and Editing, Funding acquisition. **Jinbo Bai:** Writing-Revising and Editing, Funding acquisition.

Acknowledgements

This work was supported by the National Natural Science Foundation of China (Grant Nos. 52477030, 51937007 and 51927804).

Conflict of Interest

The authors declare no conflict of interest.

References

[1] Q.-K. Feng, S.-L. Zhong, J.-Y. Pei, Y. Zhao, D.-L. Zhang, D.-F. Liu, Y.-X. Zhang, Z.-M. Dang, Recent progress and future prospects on all-organic polymer dielectrics for energy storage capacitors, Chemical Reviews 122(3) (2021) 3820-3878.

[2] X. Wu, X. Chen, Q. Zhang, D.Q. Tan, Advanced dielectric polymers for energy storage, Energy Storage Materials 44 (2022) 29-47.

[3] G. Zhang, Q. Li, E. Allahyarov, Y. Li, L. Zhu, Challenges and opportunities of polymer nanodielectrics for capacitive energy storage, ACS Applied Materials & Interfaces 13(32) (2021) 37939-37960.

[4] Z.M. Dang, J.K. Yuan, S.H. Yao, R.J. Liao, Flexible nanodielectric materials with high permittivity for power energy storage, Advanced Materials 25(44) (2013) 6334-6365.

[5] M.F. El-Kady, V. Strong, S. Dubin, R.B. Kaner, Laser scribing of high-performance and flexible graphene-based electrochemical capacitors, Science 335(6074) (2012) 1326-1330.

[6] Z. Yao, Z. Song, H. Hao, Z. Yu, M. Cao, S. Zhang, M.T. Lanagan, H. Liu, Homogeneous/inhomogeneous- structured dielectrics and their energy- storage performances, Advanced Materials 29(20) (2017) 1601727.

[7] J.S. Ho, S.G. Greenbaum, Polymer capacitor dielectrics for high temperature applications, ACS applied materials & interfaces 10(35) (2018) 29189-29218.

[8] T. Zhang, X. Chen, Y. Thakur, B. Lu, Q. Zhang, J. Runt, Q. Zhang, A highly scalable dielectric metamaterial with superior capacitor performance over a broad temperature, Science advances 6(4) (2020) eaax6622.

[9] J. Pan, K. Li, S. Chuayprakong, T. Hsu, Q. Wang, High-temperature poly (phthalazinone ether ketone) thin films for dielectric energy storage, ACS applied materials & interfaces 2(5) (2010) 1286-1289.

[10] H. Li, D. Ai, L. Ren, B. Yao, Z. Han, Z. Shen, J. Wang, L.Q. Chen, Q. Wang, Scalable polymer nanocomposites with record high- temperature capacitive performance enabled by rationally designed nanostructured inorganic fillers, Advanced Materials 31(23) (2019) 1900875.

[11] H. Li, M.R. Gadinski, Y. Huang, L. Ren, Y. Zhou, D. Ai, Z. Han, B. Yao, Q. Wang, Crosslinked fluoropolymers exhibiting superior high-temperature energy density and charge–discharge efficiency, Energy & Environmental Science 13(4) (2020) 1279-1286.

[12] S. Cheng, Y. Zhou, Y. Li, C. Yuan, M. Yang, J. Fu, J. Hu, J. He, Q. Li, Polymer dielectrics sandwiched by medium-dielectric-constant nanoscale deposition layers for high-temperature capacitive energy storage, Energy Storage Materials 42 (2021)

445-453.

[13] J. Dong, R. Hu, X. Xu, J. Chen, Y. Niu, F. Wang, J. Hao, K. Wu, Q. Wang, H. Wang, A facile in situ surface- functionalization approach to scalable laminated high- temperature polymer dielectrics with ultrahigh capacitive performance, Advanced Functional Materials 31(32) (2021) 2102644.

[14] B. Zhang, X.-m. Chen, W.-w. Wu, A. Khesro, P. Liu, M. Mao, K. Song, R. Sun, D. Wang, Outstanding discharge energy density and efficiency of the bilayer nanocomposite films with BaTiO3-dispersed PVDF polymer and polyetherimide layer, Chemical Engineering Journal 446 (2022) 136926.

[15] M.S. Islam, W.M. Chance, H.-C. zur Loye, H.J. Ploehn, Dielectric properties and energy storage performance of CCTO/polycarbonate composites: influence of CCTO synthesis route, Journal of Sol-Gel Science and Technology 73 (2015) 22-31.

[16] X. Li, Y. Xie, J. Xiong, D. Long, J. Zhang, B. Zhu, X. Zhang, X. Duan, Z. Liu, Z. Zhang, Structural tailoring enables ultrahigh energy density and charge-discharge efficiency of PAEK copolymer dielectrics at high temperatures, Chemical Engineering Journal 466 (2023) 143324.

[17] Q. Li, L. Chen, M.R. Gadinski, S. Zhang, G. Zhang, H.U. Li, E. Iagodkine, A. Haque, L.-Q. Chen, T.N. Jackson, Flexible high-temperature dielectric materials from polymer nanocomposites, Nature 523(7562) (2015) 576-579.

[18] S. Wu, W. Li, M. Lin, Q. Burlingame, Q. Chen, A. Payzant, K. Xiao, Q. Zhang, Aromatic polythiourea dielectrics with ultrahigh breakdown field strength, low dielectric

loss, and high electric energy density, Advanced Materials (Deerfield Beach, Fla.) 25(12) (2013) 1734-1738.

[19] A. Azizi, M.R. Gadinski, Q. Li, M.A. AlSaud, J. Wang, Y. Wang, B. Wang, F. Liu, L.Q. Chen, N. Alem, High- performance polymers sandwiched with chemical vapor deposited hexagonal boron nitrides as scalable high- temperature dielectric materials, Advanced Materials 29(35) (2017) 1701864.

[20] Y. Zhou, Q. Li, B. Dang, Y. Yang, T. Shao, H. Li, J. Hu, R. Zeng, J. He, Q. Wang, A scalable, high- throughput, and environmentally benign approach to polymer dielectrics exhibiting significantly improved capacitive performance at high temperatures, Advanced Materials 30(49) (2018) 1805672.

[21] S. Cheng, Y. Zhou, J. Hu, J. He, Q. Li, Polyimide films coated by magnetron sputtered boron nitride for high-temperature capacitor dielectrics, IEEE Transactions on Dielectrics and Electrical Insulation 27(2) (2020) 498-503.

[22] M. Feng, T. Zhang, C. Song, C. Zhang, Y. Zhang, Y. Feng, Q. Chi, Q. Chen, Q. Lei, Improved energy storage performance of all-organic composite dielectric via constructing sandwich structure, Polymers 12(9) (2020) 1972.

[23] M. Yang, Z. Wang, Y. Zhao, Z. Liu, H. Pang, Z.M. Dang, Unifying and Suppressing Conduction Losses of Polymer Dielectrics for Superior High- Temperature Capacitive Energy Storage, Advanced Materials (2023) 2309640.

[24] M. Fan, P. Hu, Z. Dan, J. Jiang, B. Sun, Y. Shen, Significantly increased energy density and discharge efficiency at high temperature in polyetherimide nanocomposites

by a small amount of Al_2O_3 nanoparticles, Journal of Materials Chemistry A 8(46) (2020) 24536-24542.

[25] P. Wang, Y. Guo, D. Zhou, D. Li, L. Pang, W. Liu, J. Su, Z. Shi, S. Sun, High- temperature flexible nanocomposites with ultra- high energy storage density by nanostructured MgO fillers, Advanced Functional Materials 32(31) (2022) 2204155.

[26] M. Feng, Y. Feng, C. Zhang, T. Zhang, Q. Chen, Q. Chi, Ultrahigh energy storage performance of all-organic dielectrics at high-temperature by tuning the density and location of traps, Materials Horizons 9(12) (2022) 3002-3012.

[27] M. Feng, Y. Feng, C. Zhang, T. Zhang, X. Tong, Q. Gao, Q. Chen, Q. Chi, Enhanced High- Temperature Energy Storage Performance of All- Organic Composite Dielectric via Constructing Fiber- Reinforced Structure, Energy & Environmental Materials 7(2) (2024) e12571.

[28] B. Zhang, X.m. Chen, Z. Pan, P. Liu, M. Mao, K. Song, Z. Mao, R. Sun, D. Wang, S. Zhang, Superior high- temperature energy density in molecular semiconductor/polymer all- organic composites, Advanced Functional Materials 33(5) (2023) 2210050.

[29] C. Yuan, Y. Zhou, Y. Zhu, J. Liang, S. Wang, S. Peng, Y. Li, S. Cheng, M. Yang, J. Hu, Polymer/molecular semiconductor all-organic composites for high-temperature dielectric energy storage, Nature communications 11(1) (2020) 3919.

[30] J. Li, X. Liu, B. Huang, D. Chen, Z. Chen, Y. Li, Y. Feng, J. Yin, H. Yi, T. Li, Thermally activated dynamic bonding network for enhancing high-temperature energy storage performance of PEI-based dielectrics, Materials Horizons 10(9) (2023)

3651-3659.

[31] F. Wang, J. Cai, C. Yang, H. Luo, X. Li, H. Hou, G. Zou, D. Zhang, Improved capacitive energy storage nanocomposites at high temperature utilizing ultralow loading of bimetallic MOF, Small 19(26) (2023) 2300510.

[32] J. Zhang, J. Shi, H. Zhao, J. Bai, X. Li, K. Leng, Crystal growth blocking strategy enabling efficient solvent-free synthesis of hierarchical UiO-66 for large-molecule catalysis, Crystal Growth & Design 23(2) (2023) 1205-1210.

[33] Y. Li, J. Yin, Y. Feng, J. Li, H. Zhao, C. Zhu, D. Yue, Y. Liu, B. Su, X. Liu, Metal-organic Framework/Polyimide composite with enhanced breakdown strength for flexible capacitor, Chemical Engineering Journal 429 (2022) 132228.

[34] D.X. Trinh, T.P.N. Tran, T. Taniike, Fabrication of new composite membrane filled with UiO-66 nanoparticles and its application to nanofiltration, Separation and Purification Technology 177 (2017) 249-256.

[35] J.D. Clogston, A.K. Patri, Zeta potential measurement, Characterization of nanoparticles intended for drug delivery (2011) 63-70.

[36] W. Ren, M. Yang, L. Zhou, Y. Fan, S. He, J. Pan, T. Tang, Y. Xiao, C.W. Nan, Y. Shen, Scalable ultrathin all- organic polymer dielectric films for high- temperature capacitive energy storage, Advanced Materials 34(47) (2022) 2207421.

[37] Y. Zhu, Y. Zhu, X. Huang, J. Chen, Q. Li, J. He, P. Jiang, High energy density polymer dielectrics interlayered by assembled boron nitride nanosheets, Advanced Energy Materials 9(36) (2019) 1901826.

[38] F. Chiu, Adv. Mater. Sci. Eng, Adv. Mater. Sci. Eng 2014(578168) (2014).

[39] Q. Li, F.-Z. Yao, Y. Liu, G. Zhang, H. Wang, Q. Wang, High-temperature dielectric materials for electrical energy storage, Annual Review of Materials Research 48(1) (2018) 219-243.

[40] S. Li, D. Min, W. Wang, G. Chen, Linking traps to dielectric breakdown through charge dynamics for polymer nanocomposites, IEEE Transactions on Dielectrics and Electrical Insulation 23(5) (2016) 2777-2785.

[41] D.Q. Tan, Review of polymer- based nanodielectric exploration and film scale- up for advanced capacitors, Advanced Functional Materials 30(18) (2020) 1808567.

[42] F. Liu, Q. Li, Z. Li, Y. Liu, L. Dong, C. Xiong, Q. Wang, Poly (methyl methacrylate)/boron nitride nanocomposites with enhanced energy density as high temperature dielectrics, Composites Science and Technology 142 (2017) 139-144.

[43] H. Chen, Z. Pan, W. Wang, Y. Chen, S. Xing, Y. Cheng, X. Ding, J. Liu, J. Zhai, J. Yu, Ultrahigh discharge efficiency and improved energy density in polymer-based nanocomposite for high-temperature capacitors application, Composites Part A: Applied Science and Manufacturing 142 (2021) 106266.

[44] H. Li, L. Ren, D. Ai, Z. Han, Y. Liu, B. Yao, Q. Wang, Ternary polymer nanocomposites with concurrently enhanced dielectric constant and breakdown strength for high- temperature electrostatic capacitors, InfoMat 2(2) (2020) 389-400.

[45] L. Ren, H. Li, Z. Xie, D. Ai, Y. Zhou, Y. Liu, S. Zhang, L. Yang, X. Zhao, Z. Peng, High- temperature high- energy- density dielectric polymer nanocomposites utilizing

inorganic core–shell nanostructured nanofillers, Advanced Energy Materials 11(28) (2021) 2101297.

[46] Y. Niu, J. Dong, Y. He, X. Xu, S. Li, K. Wu, Q. Wang, H. Wang, Significantly enhancing the discharge efficiency of sandwich-structured polymer dielectrics at elevated temperature by building carrier blocking interface, Nano Energy 97 (2022) 107215.

[47] K. Zhang, Z. Ma, Q. Fu, H. Deng, Multi-layered boron nitride/polyimide high-temperature capacitor dielectric film, Materials Today Energy 29 (2022) 101093.

[48] T. Zhang, L. Yang, C. Zhang, Y. Feng, J. Wang, Z. Shen, Q. Chen, Q. Lei, Q. Chi, Polymer dielectric films exhibiting superior high-temperature capacitive performance by utilizing an inorganic insulation interlayer, Materials Horizons 9(4) (2022) 1273-1282.

[49] J. Liu, L. Ji, J. Yu, S. Ding, S. Luo, B. Chu, J. Xu, R. Sun, S. Yu, Enhanced breakdown strength and electrostatic energy density of polymer nanocomposite films realized by heterostructure ZnO-ZnS nanoparticles, Chemical Engineering Journal 456 (2023) 140950.

[50] C. Yan, Y. Wan, H. Long, H. Luo, X. Liu, H. Luo, S. Chen, Improved Capacitive Energy Storage at High Temperature via Constructing Physical Cross- Link and Electron–Hole Pairs Based on P- Type Semiconductive Polymer Filler, Advanced Functional Materials 34(8) (2024) 2312238.

[51] Y. Wang, Z. Li, T.J. Moran, L.A. Ortiz, C. Wu, A.C. Konstantinou, H. Nguyen, J. Zhou, J. Huo, K. Davis- Amendola, Interfacial 2D montmorillonite nanocoatings enable sandwiched polymer nanocomposites to exhibit ultrahigh capacitive energy storage

performance at elevated temperatures, Advanced Science 9(35) (2022) 2204760.

[52] J. Yu, L. Wang, Z. Liang, P. Xu, Y. Min, Z. Liu, J. Huang, S. Luo, S. Yu, R. Sun, Elaborately designed polymer dielectric films with low coefficient of thermal expansion demonstrating high and stable electrostatic energy density over a wide temperature range, Materials Today Energy 30 (2022) 101177.

[53] L. Ren, L. Yang, S. Zhang, H. Li, Y. Zhou, D. Ai, Z. Xie, X. Zhao, Z. Peng, R. Liao, Largely enhanced dielectric properties of polymer composites with HfO_2 nanoparticles for high-temperature film capacitors, Composites Science and Technology 201 (2021) 108528.